Pergamon

Journal of Structural Geology, Vol. 17, No. 10, pp. 1407 to 1423, 1995

0191-8141/95 $9.50+0.00

0191-8141(95)00039-9

Effect of deformation on oxygen isotope exchange in the Heavitree Quartzite, Ruby Gap duplex, central Australia

DAVID L. KIRSCHNER,* CHRISTIAN TEYSSIER*

Department of Geology and Geophysics, University of Minnesota, Minneapolis, MN 55455, U.S.A.

ROBERT T. GREGORY

Department of Geological Sciences, Southern Methodist University, Dallas, TX 75275, U.S.A.

and

ZACHARY D. SHARP

Université de Lausanne, Institut de Minéralogie et Pétrographie BFSH-2, CH-1015 Lausanne, Switzerland

(*Received* 13 *May* 1994; *accepted in revised form* 18 *March* 1995)

Abstract—$\delta^{18}O$ values of the Heavitree Quartzite, central Australia, vary systematically as a function of deformation and recrystallization in a duplex composed of 5 superposed thrust sheets which formed under greenschist-grade conditions. Undeformed quartzite of the basal thrust sheet 1 and moderately strained and partially recrystallized quartzite of thrust sheet 2 range over 4‰ in $\delta^{18}O$ values and have an average value of ~12.8‰. Entirely recrystallized quartzite of overlying thrust sheet 3 retains a similar average value of ~12.3‰ but shows a narrow range of ~1.5‰, suggesting isotopic homogenization. Recrystallized quartzites of sheet 5 have a lower $\delta^{18}O$ value than the other thrust sheets. The homogenized $\delta^{18}O$ values of sheet 3 relative to sheets 1 and 2 could not have resulted from mechanical mixing, isotopic exchange during dissolution-reprecipitation, or exchange by diffusion between the quartzite and a fluid in microfractures or along grain boundaries. The homogenized $\delta^{18}O$ values of sheet 3 and lowered values of sheet 5 are interpreted to have been produced by isotopic exchange during recrystallization by grain-boundary migration. This is probably an important mechanism of isotopic exchange for rocks undergoing dynamic recrystallization.

INTRODUCTION

The progressive deformation of quartzite under greenschist-grade conditions involves processes of fracturing, mass-transfer and dislocation creep, the predominance of which may change for any rock body during the course of a single orogenic event. These processes create, alter, or destroy fluid pathways and, consequently, may have profound effects on isotopic exchange between any fluid present and the deforming rock.

In this paper we correlate the deformation-related microstructures preserved in the Heavitree Quartzite, central Australia, with the measurements of oxygen-isotope values, and attempt to identify the processes responsible for isotopic exchange. The Heavitree Quartzite has experienced only one deformation event and exhibits a range of microstructures that are spatially arranged within the Ruby Gap mid-crustal duplex. Relatively undeformed quartzite is preserved in unconformable contact with the basement in the foreland of the duplex. Within the duplex, dissolution seams and microfractures are the dominant microstructure in the least deformed thrust sheet, and the quartzite is entirely recrystallized in the most deformed sheets. This systematic spatial distribution of microstructures in the duplex is interpreted to reflect the microstructural history for individual thrust sheets.

The variation in isotopic composition of the quartzite within the duplex is used to determine the extent of fluid migration through the thrust system and the local scale of homogenization attending deformation. Though all possible microstructural transformations may have facilitated isotopic exchange, dynamic recrystallization by grain-boundary migration had the most pronounced effect on isotopic exchange within the quartzite of the duplex.

GEOLOGY

The mid-crustal Ruby Gap duplex forms a portion of the Arltunga Nappe Complex where south-directed thrusting intercalated felsic and mafic basement gneisses metamorphosed to amphibolite and granulite facies in Early Proterozoic time, with upper Proterozoic–Paleozoic supracrustal sedimentary strata (Forman *et al.* 1967, Forman 1971, Stewart 1971, Shaw *et al.* 1971, Yar Khan 1972, Teyssier 1985, Kirschner & Teyssier 1992,

*Present address: Université de Lausanne, Institut de Minéralogie et Pétrographie BFSH-2, CH-1015 Lausanne, Switzerland.

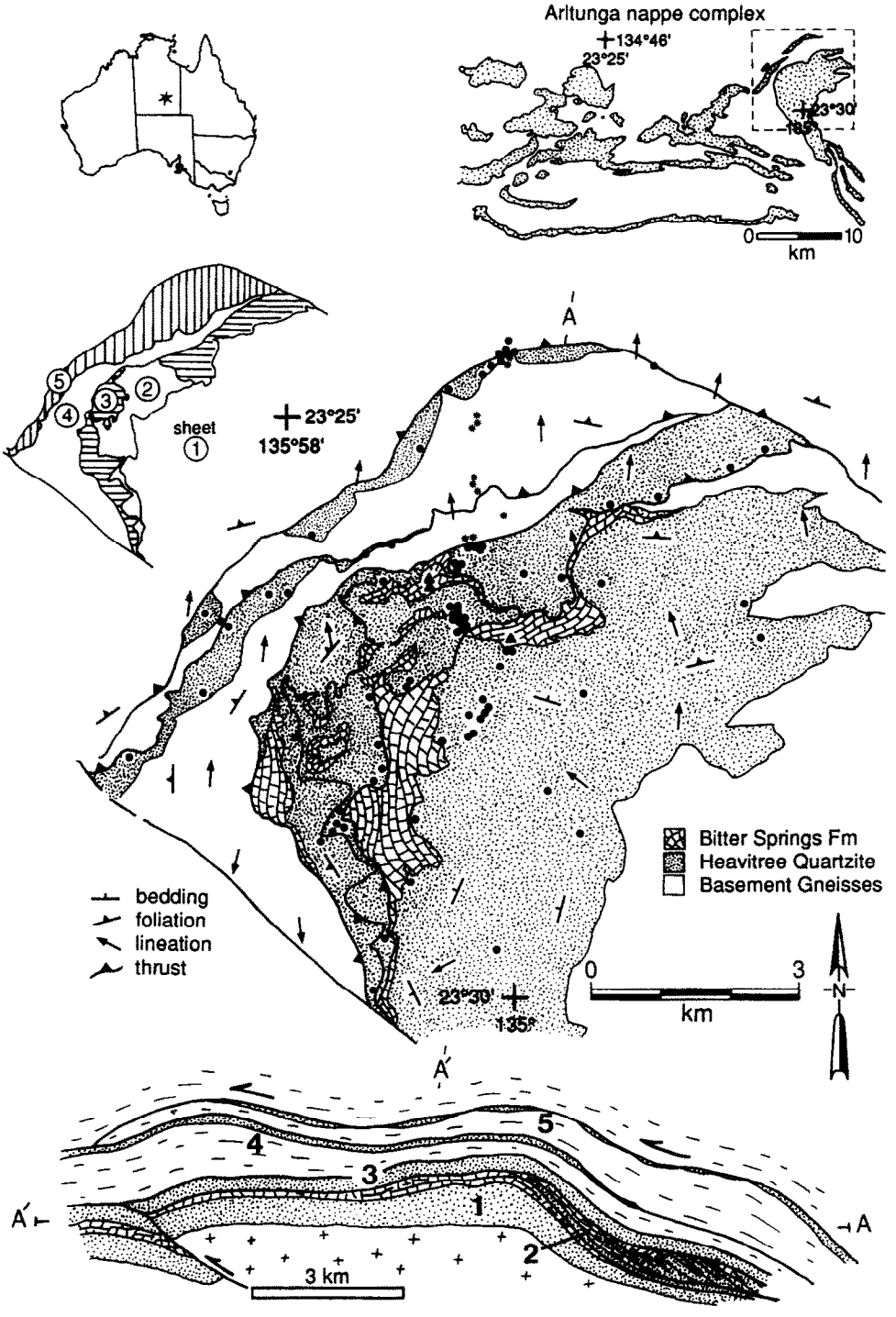

Fig. 1. Structure map and cross-section of Ruby Gap duplex, Arltunga nappe complex, central Australia. *S*-directed thrusting interleaved felsic and mafic basement gneisses with supracrustal Heavitree Quartzite and Bitter Springs carbonate to form antiformal duplex composed of five thrust sheets (sheet 1 parautochthonous). Samples analyzed in this study for their oxygen isotope values are shown in the map as circles (quartzite), triangles (carbonate), and stars (basement gneisses). Map and cross section (no vertical exaggeration) reproduced with permission from Dunlap (1992).

Dunlap 1992, Dunlap *et al.* in press). The basement in the hinterland of the orogen was substantially uplifted and moved southward along anastomosing networks of N-dipping ductile faults (Collins & Teyssier 1989). The sedimentary strata in the foreland of the orogen were folded and thrust southward along N-dipping ductile and brittle thrusts.

The 100 km^2 Ruby Gap duplex is composed of five major thrust sheets (Fig. 1). Parautochthonous sheet 1, the lowermost thrust sheet, is composed of gneissic basement unconformably overlain by Heavitree Quartzite, which is in turn overlain by Bitter Springs Formation carbonate, siltstone, and evaporite. Sheet 2 is composed only of Heavitree Quartzite and Bitter Springs Formation. Sheet 3 consists exclusively of Heavitree Quartzite. Sheets 4 and 5 are composed of gneissic basement

overlain by thin veneers of Heavitree Quartzite. Formation and deformation of the duplex occurred over a 20 Ma period, from 330–310 Ma (Dunlap *et al.* 1991, Dunlap 1992). Structures and microstructures within the Ruby Gap Duplex have been mapped and studied in detail by Dunlap (1992) and Dunlap *et al.* (in press).

Rocks within basement shear zones in the nappe complex are retrograded to the greenschist facies in the south and the epidote–albite amphibolite facies in the north. Correspondingly, the supracrustal sediments are metamorphosed to the greenschist facies in the Ruby Gap duplex. $^{40}Ar/^{39}Ar$ analyses of neoformed phengites in Ruby Gap yield a Devonian–Carboniferous age, while detrital muscovite preserves a Proterozoic age. The lack of reequilibration by the detrital muscovite constrains a maximum temperature of less than approximately 350–400°C (i.e. the closure temperature of argon in muscovite) for the formation of the duplex (Dunlap *et al.* 1991, Dunlap 1992). Oxygen-isotope thermometry of quartz and neoformed micas from sheets 3 and 5 yield temperatures of 330–400°C, respectively.

Mesoscopic structures

Parautochthonous sheet 1 is undeformed to weakly deformed. A weak N-dipping foliation, defined by neoformed phengite, is present in much of this sheet. This foliation is more pronounced in thin (<1 m) phyllitic horizons and in more massive quartzite near the thrust at the base of sheet 2. Cross-beds and ripple marks are well preserved within thickly bedded horizons of sheet 1. Slickensides with N–S oriented striae are present on some bedding planes and on steeply-dipping fracture surfaces. The striae are defined either by precipitated quartz fibers or by rotated, elongated, and partially recrystallized quartz porphyroclasts. The quartzite of sheet 1 contains numerous en échelon quartz vein arrays whose orientations are consistent with formation during north-over-south thrusting. The overlying carbonate-clastic Bitter Springs Formation is moderately deformed and folded.

Allochthonous sheet 2 is moderately to strongly deformed. The base of sheet 2 is composed of a well-foliated quartzite overlain by an isoclinally folded and imbricated package of quartzite and carbonate. Within this sheet, a moderately well-developed foliation is defined by flattened quartz and neocrystallized phengite. A prominent N–S trending lineation is defined by elongated quartz grains. Within the quartzite of sheet 2, there are many small *S*-directed, bedding-parallel shear zones which contain N-dipping quartz veins subparallel to the foliation. The numerous veins outside the shear zones are more steeply inclined to the foliation. Most of these veins are sigmoidal and consistent with north-over-south thrusting. Few well-developed slickensides are preserved in the bedding-parallel shear zones of sheet 2. Large, tight folds on the order of 5–15 m wavelength are present within both the Heavitree Quartzite and Bitter Springs Formation of sheet 2.

The entirely recrystallized quartzite of sheets 3, 4 and 5 contains a well-developed mylonitic foliation and N-trending lineation. The most prominent mesoscopic features of these thrust sheets, apart from the mylonitic foliation, are N-dipping deformed and recrystallized veins that crosscut the foliation at a low angle. These veins are locally boudinaged. Most of these deformed veins are subparallel to the mylonitic foliation, suggesting that they formed early in the deformation history and were subsequently rotated and deformed. There are very few veins in sheets 3–5 that crosscut the mylonitic foliation at moderate to high angles.

Microstructures

The quartzite of Ruby Gap contains a wide range of microstructures, which vary systematically from the relatively undeformed sheet 1 to the entirely recrystallized sheets 3–5 (Fig. 2). Most of the quartzite of sheet 1 exhibits pressure-solution microstructures that resulted from preferential removal of quartz along N-dipping grain contacts. The preferred orientation of these straight grain boundaries in quartz, along with the alignment of millimeter-size detrital muscovites and small neoformed phengites, produce the weak N-dipping foliation (Dunlap *et al.* 1991, Dunlap 1992). The millimeter(s)-size detrital quartz grains of sheet 1 contain undulatory extinction, deformation bands, and small recrystallized quartz grains which mantle the quartz porphyroclasts. Based on the microstructural comparison of experimentally deformed Heavitree Quartzite (Hirth & Tullis 1992) with the Heavitree Quartzite of Ruby Gap, Hirth *et al.* (1991) and Dunlap (1992) suggested that the dislocation-related microstructures of sheet 1 quartzite are consistent with dislocation climb having been inoperative and with recovery dominated by grain-boundary migration recrystallization during deformation (i.e. regime 1 of Hirth & Tullis 1992). Quartz *c*-axes in sheet 1 quartzite are randomly oriented, typical of relatively undeformed sandstone and quartzite (Fig. 4).

The northern part of sheet 1 and the entirety of sheet 2 show flattened and elongated quartz grains, surrounded by fine-grained recrystallized quartz and white mica (Fig. 2b). In addition, undulatory extinction, deformation bands and lamellae, subgrains and recrystallized grains are ubiquitous. These microstructures are consistent with climb processes having been efficient during deformation and recrystallization dominated by subgrain rotation (i.e. regime 2 of Hirth & Tullis 1992, Hirth *et al.* 1991, Dunlap 1992). The preferred orientations of quartz *c*-axes in sheet 2 define cross-girdle patterns indicative of increased dislocation-related deformation relative to the less deformed quartzite of sheet 1 (Fig. 4).

In sheet 3, the quartzite is entirely recrystallized, with an average grain size of 80 μm. Within sheets 4 and 5, the quartzite is entirely recrystallized with grain sizes up to 100–150 μm (Dunlap 1992). The quartz microstructure of sheet 3 is characterized by a grain shape fabric of the recrystallized grains whose long axes are inclined to the mica foliation plane consistent with a southward sense-

of-shear (Lister & Snoke 1984, Burg 1986). White micas of sheet 3 are located along quartz grain boundaries and heterogeneously distributed in the quartzite mylonite such that mica-rich zones anastomose around pure, ellipsoidal quartz domains. These pure quartz domains are interpreted to be recrystallized relicts of quartz porphyroclasts in the quartzite, though in some cases they are rotated, recrystallized quartz veins.

Although the asymmetric quartz grain-shape and crystallographic fabric is also present in the quartzite of sheets 4 and 5, quartz grains are more commonly equant with gently curving to straight grain boundaries that locally form ~120° triple junctions. The more equant white mica is not restricted to quartz grain boundaries, such as in sheet 3 quartzite, but is commonly contained within quartz grains and homogeneously distributed in the quartzite mylonite. Hirth *et al.* (1991) and Dunlap (1992) have suggested the quartz microstructure is consistent with dislocation-climb dominated recovery and recrystallization dominated by grain-boundary migration (i.e. regime 3 of Hirth & Tullis 1992). The preferred orientations of quartz *c*-axes in sheets 3 and 5 (Fig. 4) clearly define single and cross-girdle patterns (Bouchez *et al.* 1983), which are inclined toward the foliation, consistent with the kinematics of *S*-directed thrusting. The systematic increase in quartz fabric intensity from sheet 1 to sheet 5 indicates the increased role of dislocation-related mechanisms in the deformation of the Heavitree Quartzite from the base to the roof of the duplex.

Microfractures and veins

Sealed microfractures, as evidenced by secondary fluid inclusion planes, are common in the quartzite porphyroclasts, but are rarely present in the recrystallized quartz grains of thrust sheets 1 and 2. The inclusion planes in general dip steeply to the south, an orientation consistent with extensional formation during *S*-directed thrusting. The inclusion planes are usually spaced on the order of 100–200 μm, but have spacings as small as 10 μm in the vicinity of mesoscopic quartz veins. Though some inclusion planes can be traced across several adjacent porphyroclasts, most inclusion planes within individual clasts are not obviously aligned with or related to inclusion planes in neighboring clasts. In both cases, inclusion planes within clasts do not continue into the intervening recrystallized quartz matrix. Intragranular and transgranular secondary fluid inclusion planes are absent in the entirely recrystallized quartzite mylonites of sheets 3, 4 and 5.

The absence of fluid inclusion planes in the recrystallized quartz grains of sheets 1 and 2, and in the quartzite mylonites of sheets 3, 4 and 5, can be explained in several ways. One possibility is that the majority of microfractures developed prior to, and were subsequently destroyed by, grain-boundary migration recrystallization (cf. Kerrich 1976). Alternatively, microfractures contemporaneous with recrystallization may have localized along grain boundaries in the finer-grained recrystallized quartz aggregates rather than within or across individual grains.

Although the relative timing between microfracturing and recrystallization in the quartzite cannot be definitively reconstructed, three observations are consistent with the inference that the majority of microfractures and veins formed early in the deformation history of each thrust sheet and subsequently were overprinted by recrystallization. First, the nappe complex as a whole formed by foreland propagation and imbrication (Dunlap *et al.* 1991, Dunlap 1992) with a corresponding increase in finite strain, ductile deformation, and dynamic recrystallization from foreland to hinterland (Yar Khan 1972, Kirschner & Teyssier 1992, Dunlap 1992). Secondly, inclusion planes are present only within the partially recrystallized thrust sheets 1 and 2 of the duplex and not within the entirely recrystallized sheets 3, 4 and 5. Thus microfractures did not overprint the mylonitic fabrics (e.g. during exhumation of the duplex) but are related to the formation of the duplex. Finally, veins are undeformed to moderately deformed and oriented oblique to the quartzite foliation in the less deformed thrust sheets 1 and 2, whereas the veins of sheets 3–5 are highly deformed and subparallel to the mylonitic fabric.

Temporal evolution of microstructures

The Heavitree Quartzite has experienced only one orogeny; therefore, deformation and microstructural transformations of the quartzite must have developed during this event. We infer the temporal evolution of structures for individual thrust sheets by assuming foreland imbrication of thrust sheets during duplex development (Boyer & Elliott 1982) and by considering the documented systematic spatial distribution of structures and microstructures. During the early stages of duplex development, structures and microstructures of sheet 5 quartzite would initially have resembled the structures and microstructures currently observed in sheet 1 quartzite. The structures and microstructures of sheet 5 would have sequentially progressed to resemble those of sheet 2, then 3 and then sheet 4 quartzite with subsequent deformation and imbrication of new thrusts. The amount of fracturing and grain-shape change of detrital grains prior to recrystallization, however, might have varied for each thrust sheet. This microstructural evolution is similar to that documented by Yar Khan (1972), Marjoribanks (1976), and Kirschner & Teyssier (1992) for the Heavitree Quartzite incorporated into other duplex-like structures developed in the same orogen. This spatial and temporal evolution of the structures and microstructures in the duplex will be used as a framework for understanding the oxygen isotope data recorded in the duplex.

RESULTS OF ISOTOPIC ANALYSES

Stable isotope analyses were made using both conventional and laser-based techniques (see Appendix 1 for

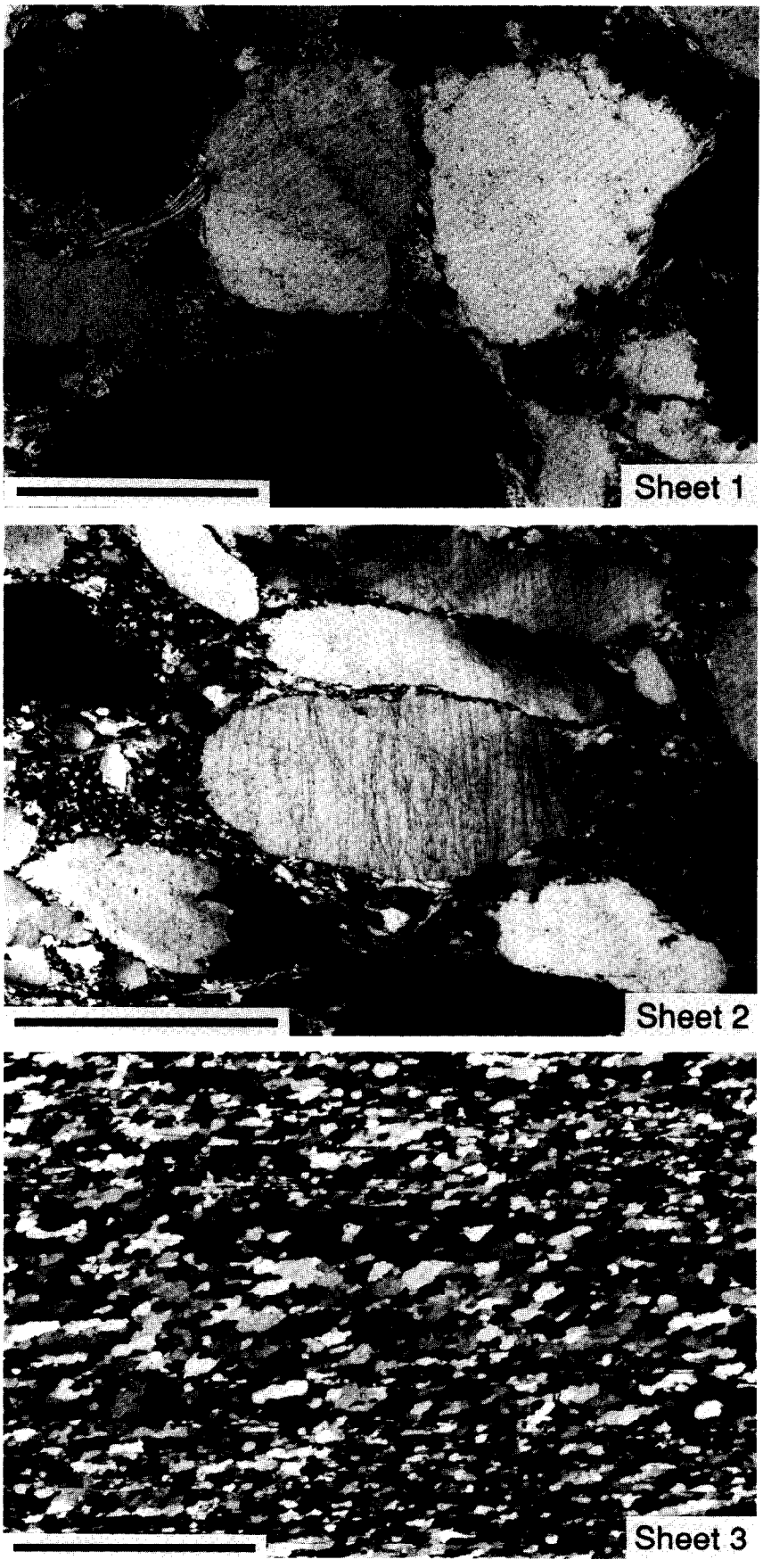

Fig. 2. Heavitree Quartzite microstructures in Ruby Gap duplex. Sheet 1 quartzite (SI58) is mildly deformed with local preservation of 'dust' rims and quartz cement. Small, recrystallized quartz grains mantle the detrital grains. Fine-grained phengite defines weak foliation (scale bar = 0.4 mm). Sheet 2 quartzite (R768C) is moderately strained, partially recrystallized, and extensively microfractured. Homogeneously flattened detrital grains are surrounded by recrystallized grains which frequently exhibit a grain shape fabric (scale bar = 1 mm). Sheet 3 quartzite (SI15) is entirely recrystallized and exhibits a grain shape fabric oblique to the dominant mica foliation consistent with north-over-south thrusting (scale bar = 1 mm).

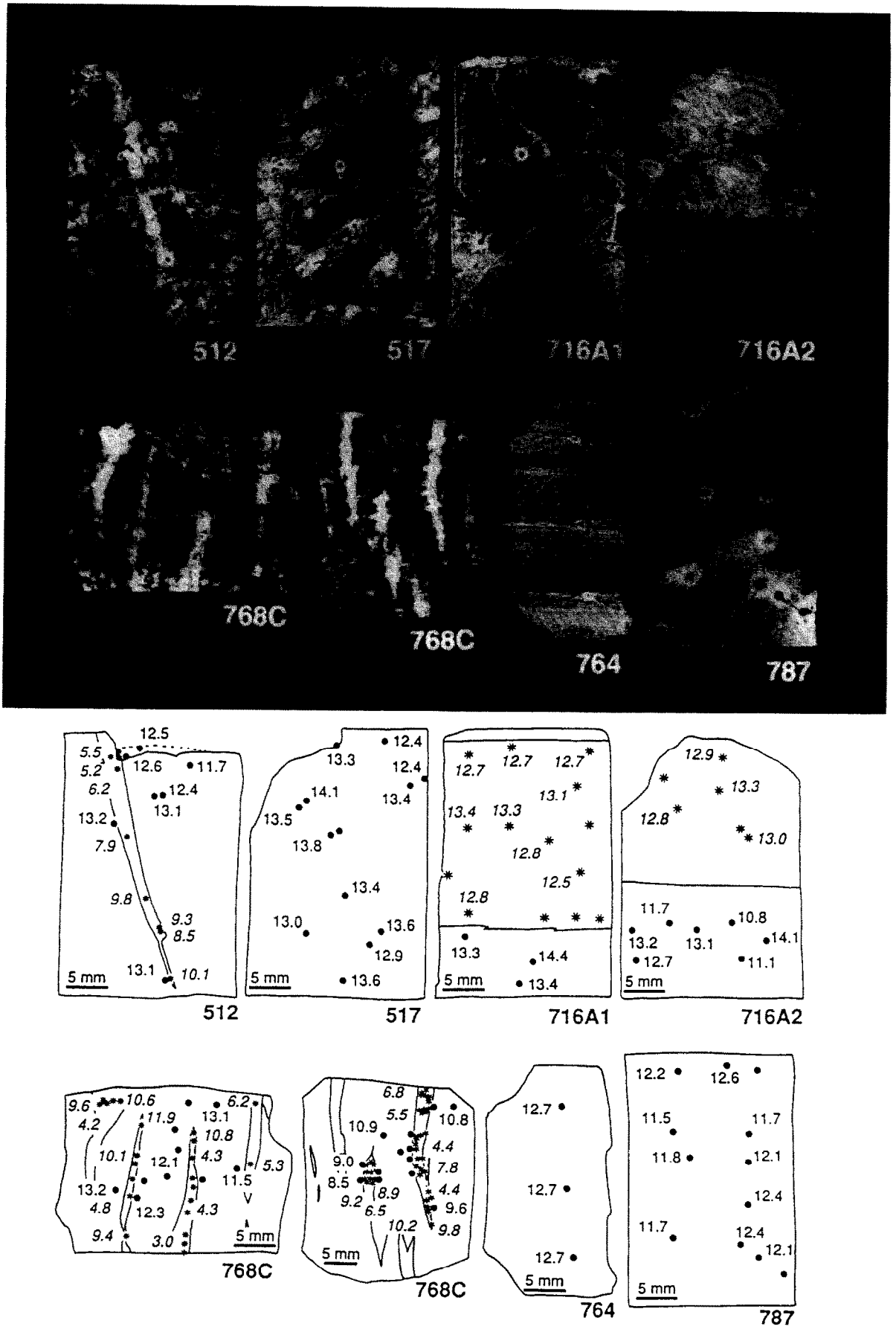

Fig. 3. $\delta^{18}O$ values obtained *in situ* on polished thick sections using laser-based extraction method (solid dots depict analyses in quartzite, stars in quartz veins). Top four samples are from sheet 1; 768C is from sheet 2; entirely recrystallized sample 764 is from sheet 3; and entirely recrystallized sample 787 is from sheet 5. Additional analyses of sample 768C are reported in Kirschner *et al.* (1993).

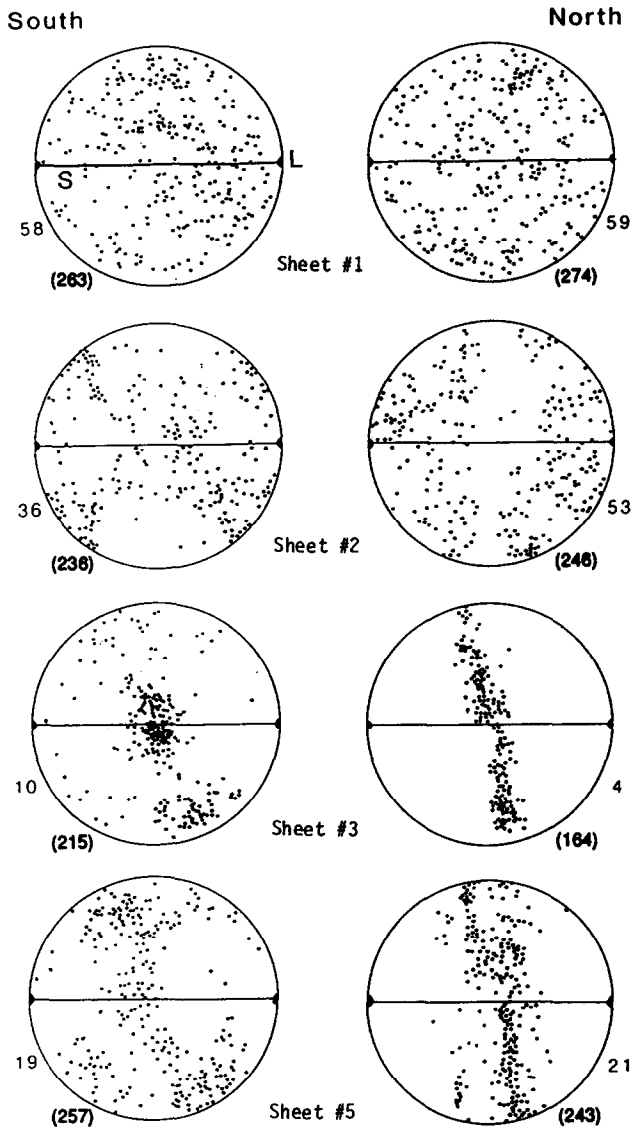

Fig. 4. Quartz *c*-axis crystallographic fabrics from Ruby Gap duplex plotted on lower hemisphere Schmidt nets. The number of *c*-axes is in parentheses and the sample numbers are the same as the SI numbers in Table 1. Increasing definition of fabrics from sheet 1 randomly oriented pattern to sheets 3 and 5 well-defined single- and cross-girdle fabrics is correlative with increasing finite strain accommodated by dislocation-related processes in quartzite of sheets 2, 3 and 5. Asymmetry between fabrics and foliation is consistent with kinematics of south-directed thrusting.

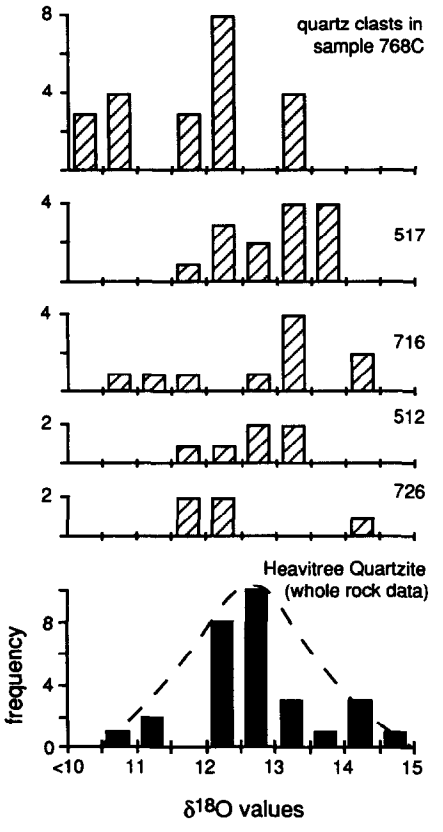

Fig. 5. $\delta^{18}O$ values of Heavitree Quartzite whole rock samples (lowest histogram) and individual quartz porphyroclasts from five samples from thrust sheets 1 and 2. Heterogeneity in $\delta^{18}O$ values in whole rock and clast populations reflects variable sedimentary mixing of quartz of igneous and metamorphic origin. Deformation has not altered or homogenized protolith $\delta^{18}O$ values in these two thrust sheets.

details). The $\delta^{18}O$ values vary systematically within the duplex (Figs. 3, 5 and 6; Table 1).

Thrust sheets 1 and 2

Quartzite of sheet 1 has an average $\delta^{18}O$ value of 12.7‰ ($1\sigma = 0.9$‰, $n = 14$ samples), while that of sheet 2 is 13.0‰ ($1\sigma = 1.0$‰, $n = 15$, Fig. 6). Individual quartz porphyroclasts in four samples from the same two thrust sheets have an average value of 12.8‰ ($1\sigma = 0.9$‰, $n = 42$). These $\delta^{18}O$ values are typical of sandstones composed of variable amounts of igneous and metamorphic quartz. The large 4‰ variation in the $\delta^{18}O$ values is thought to be representative of the undeformed Heavitree Quartzite protolith, with isotopic heterogeneity on both the hand-sample (Fig. 5) and outcrop scale. This isotopic heterogeneity might reflect variable sedimentary mixing of quartz from the Proterozoic granite–gneiss provenance (Clarke 1979) prior to deposition of the Heavitree Quartzite.

Quartz veins and fault slickenfibres from these two sheets have an average $\delta^{18}O$ value of 13.0‰ ($1\sigma = 1.1$‰, $n = 14$). The similarity in values between the quartzite and these veins are consistent with the fluids having been rock-buffered and fluid advection having been predominantly contained within individual stratigraphic units (cf. Gray *et al.* 1991). The lower δD value of sheet 1 recrystallized muscovite ($\delta D = -83$‰) to those values obtained from white mica in the overlying sheets (δD between −59‰ and −67‰, Table 1) is consistent with minor incursion of meteoric fluid into thrust sheet 1 (Table 1, Frey *et al.* 1976).

The calcite and dolomite of the Bitter Springs Formation of sheets 1 and 2 have $\delta^{18}O$ values between 21 and 24‰: these values are typical for unaltered sedimentary carbonate (e.g. Keith & Weber 1964). If the carbonate and quartzite had completely equilibrated in sheets 1 and 2 under greenschist-grade conditions ,the carbonate $\delta^{18}O$ values would be approximately 2 to 3‰ lower than those of the quartzite, instead of being ~10‰ higher as observed. In addition, a quartz-rich siltstone from the same Bitter Springs unit also retains a $\delta^{18}O$ value ~8‰ higher than the quartzite, indicative of isotopic disequili-

Table 1. Isotope data of Ruby Gap Samples (excluding data presented in Fig. 3)

Sample	Powder*	Rock Type	$\delta^{18}O$†	Method‡	Location§
Sheet 1					
R127	Qz	Quartzite	12.5	L	UL
R137	Qz	Quartzite	12.4	L	UL
R227	Qz	Quartzite	12.3	L	UL
R511	Qz	Quartzite	12.4	L	UL
R517	Qz	Quartzite	12.9	L	UL
	Qz	Porphyroclast	14.0	L	UL
	Qz	Porphyroclast	13.7	L	UL
	Qz	Porphyroclast	12.3	L	UL
	Qz	Porphyroclast	12.5	L	UL
	Qz	Porphyroclast	11.6	L	UL
R518	Qz	Quartzite	12.4	L	UL
R707	Wr	Quartzite	10.8	L	UL
R716A2	Qz	Quartzite	12.9	L	UL
R726	Qz	Quartzite	12.6	L	UL
	Qz	Porphyroclast	12.3	L	UL
	Qz	Porphyroclast	14.4	L	UL
	Qz	Porphyroclast	11.9	L	UL
	Qz	Porphyroclast	12.5	L	UL
	Qz	Porphyroclast	11.8	L	UL
R728	Qz	Quartzite	13.0	L	UL
R751	Qz	Quartzite	13.3	L	UL
SI57	Wr	Qtz cobble	15.1	C	MU
SI58	Wr	Quartzite	12.9	C	MU
SI59	Wr	Quartzite	12.5	C	MU
R100	Wr	Siltstone	20.5	C	MU
AN26	Cc	Bitter Springs	22.2	A	MU
	Do		21.2	A	MU
R694A	Qz	Vein	11.3	L	UL
R716A3	Qz	Vein	13.6	L	UL
R716D	Qz	Vein-older	12.3	L	UL
R716D	Qz	Vein-younger	12.0	L	UL
R716D1	Qz	Vein	12.2	L	UL
R716G3	Qz	Vein	15.9	L	UL
R520	Ph	Neocrystallized	$\delta D = -83‰$		UL
Sheet 2					
R218	Qz	Quartzite	11.1	L	UL
R696	Qz	Quartzite	14.5	L	UL
R697	Qz	Quartzite	13.2	L	UL
R703	Qz	Quartzite	14.3	L	UL
R704	Qz	Quartzite	12.8	L	UL
R710A	Wr	Quartzite	12.5	L	UL
R768A	Qz	Quartzite	12.7	L	UL
R768C	Qz	Quartzite	12.8	L	UL
SI36	Wr	Quartzite	13.7	C	MU
SI39	Wr	Quartzite	14.2	C	MU
SI42	Wr	Quartzite	13.0	C	MU
SI45	Wr	Quartzite	11.3	C	MU
SI48	Wr	Quartzite	13.0	C	MU
SI52	Wr	Quartzite	13.3	C	MU
SI53	Wr	Quartzite	12.4	C	MU
AN31	Cc	Bitter Springs	23.8	A	MU
	Do		21.5	A	MU
SI35	Do	Bitter Springs	23.6	A	MU
R696C	Qz	Vein	13.6	L	UL
R699B	Qz	Vein	13.5	L	UL
R700A	Qz	Vein	13.0	L	UL
R701B	Qz	Vein	12.7	L	UL
R702C	Qz	Vein	12.6	L	UL
R703B	Qz	Vein	13.3	L	UL
R767B	Qz	Vein	13.3	L	UL
R768B	Qz	Vein	13.0	L	UL
Sheet 3					
R713	Wr	Quartzite	11.8	L	UL
R750	Wr	Quartzite	12.6	L	UL
R758	Wr	Quartzite	12.6	L	UL
R759	Wr	Quartzite	12.0	L	UL
R760	Wr	Quartzite	12.2	L	UL
R764	Wr	Quartzite	12.1	L	UL
R764A	Wr	Quartzite	12.5	L	UL
SI4	Wr	Quartzite	12.4	C	MU

Continued

Table 1. Continued

Sample	Powder*	Rock Type	$\delta^{18}O$†	Method‡	Location§
SI7	Wr	Quartzite	12.3	C	MU
SI9	Wr	Quartzite	12.3	C	MU
SI10	Wr	Quartzite	12.3	C	MU
SI11	Wr	Quartzite	8.2	C	MU
R705B	Qz	Vein	13.1	L	UL
R744B	Qz	Vein	12.7	L	UL
R756B	Qz	Vein	12.0	L	UL
R764B	Qz	Vein	12.7	L	UL
R764	Ph	Neocrystallized	$\delta D = -67‰$	$\delta O = 7.6‰$	UL
Sheet 4					
R222	Wr	Quartzite	10.9	L	UL
R224	Wr	Quartzite	11.8	L	UL
R240	Wr	Quartzite	12.8	L	UL
R648C	Wr	Quartzite	12.8	L	UL
R652	Wr	Quartzite	12.8	L	UL
R648B	Qz	Vein	12.3	L	UL
R649K	Qz	Vein	12.6	L	UL
SI28	Wr	Felsic Gneiss	8.6	C	MU
SI29	Wr	Felsic Gneiss	9.4	C	MU
SI30	Wr	Felsic Gneiss	8.4	C	MU
Sheet 5					
R246	Wr	Quartzite	12.7	L	UL
R248	Wr	Quartzite	9.4	L	UL
R644	Wr	Quartzite	12.1	L	UL
R649A	Wr	Quartzite	11.8	L	UL
R649E	Wr	Quartzite	10.6	L	UL
R797B	Q-rich	Quartzite	11.7	L	UL
R781A	Wr	Quartzite	11.8	L	UL
SI16	Wr	Quartzite	10.8	C	MU
SI17	Wr	Quartzite	10.8	C	MU
SI19	Wr	Quartzite	10.7	C	MU
SI21	Wr	Quartzite	11.3	C	MU
R785B	Qz	Vein	10.3	L	UL
SI15	Qz	Vein	10.4	C	MU
SI22	Wr	Felsic Gneiss	8.5	C	MU
SI23	Wr	Felsic Gneiss	7.8	C	MU
SI24	Wr	Felsic Gneiss	8.5	C	MU
SI25	Wr	Felsic Gneiss	8.4	C	MU
SI26	Wr	Malfic gneiss	6.0	C	MU
SI27A	Wr	Mafic gneiss	6.0	C	MU
SI27B	Wr	Felsic Dike	6.0	C	MU
SI27C	Wr	Biotite Gneiss	4.0	C	MU
R796	Qz	Felsic Pegmatite	9.9	L	UL
R787	Wr	Quartzite	11.6	L	UL
R787A	Qz	Vein	11.5	L	UL
R533	Qz	Quartzite	13.6	L	UL
R797B	Mu	Neocrystallized	$\delta D = -62‰$	$\delta O = 7.9‰$	UL
R533	Ph	Neocrystallized		$\delta O = 9.6‰$	UL
R796	Mu	Proterozoic age	$\delta D = -59‰$	$\delta O = 6.7‰$	UL

*Designations: Qz = quartz separate, Ph = phengite, Mu = muscovite, Cc = calcite, Do = dolomite, Wr = whole rock.

†Values corrected relative to the results of internal laboratory quartz standard, which was analyzed with samples.

‡Extraction method employed: L = laser ablation method; C = conventional fluorination method; A = acid digestion.

§UL = Analyzed at University of Lausanne; MU = Monash University.

brium between these two rock types. The large isotopic disequilibrium is consistent with no appreciable isotopic exchange between the sheet 1 quartzite and the carbonate/clastic Bitter Springs Formation. There was possibly very limited exchange between sheet 2 quartzite and its bounding carbonate, which would account for the slightly heavier isotopic values of sheet 2 relative to sheet 1 quartzite.

Thrust sheet 3

Sheet 3 quartzite has an average $\delta^{18}O$ value of 12.3‰ ($1\sigma = 0.2‰$, $n = 11$ excluding sample SI11), and quartz veins have a mean value of 12.6‰ ($1\sigma = 0.5‰$, $n = 4$). Although these mean values are similar to those of sheet 1 and 2 quartzite and veins, the range in values for the quartzite and quartz veins of sheet 3 is significantly less

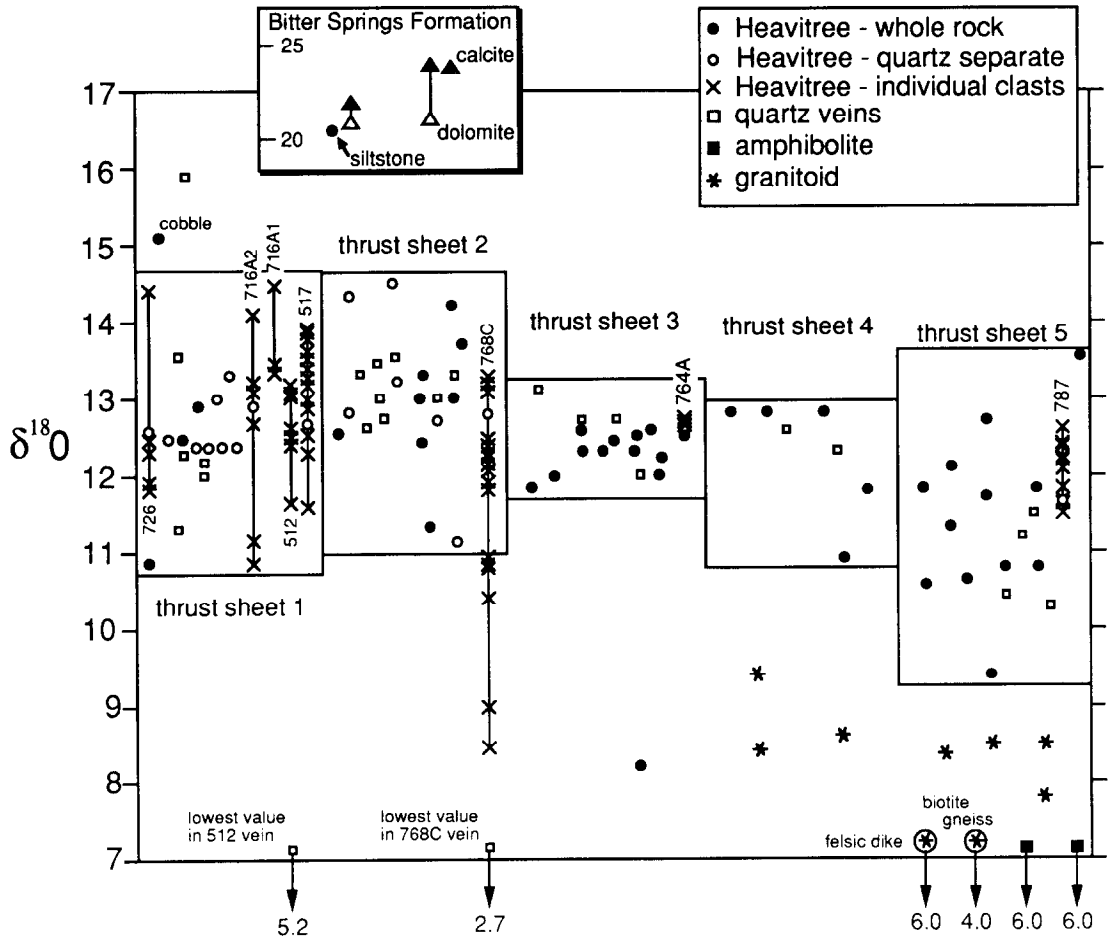

Fig. 6. $\delta^{18}O$ values of quartzite, quartz veins, and basement gneisses from Ruby Gap duplex. Within each individual thrust sheet, the data are horizontally arranged left-to-right according to relative position in the duplex, from south to north. Boxes bracket the quartzite whole rock and quartz separate $\delta^{18}O$ values.

than in sheets 1 and 2 (Fig. 6). The similarity in mean values would be consistent with the deformation occurring in an isotopically-closed system with no significant isotopic exchange between the quartzite and the overlying basement gneisses of sheet 4, underlying carbonate of sheet 2, or meteoric fluids. This conclusion is supported by the δD value of $-67‰$ obtained for syntectonically recrystallized muscovite from this thrust sheet. This δD value is in the typical range for metamorphic muscovite that has not isotopically exchanged with meteoric fluids at elevated temperatures (cf. fig. 8 in Sharp *et al.* 1993). The reduced range in $\delta^{18}O$ values is consistent with isotopic homogenization having occurred within sheet 3 during deformation, assuming the original undeformed quartzite of sheet 3 had a similar spread in $\delta^{18}O$ values as sheets 1 and 2 quartzite.

Thrust sheet 4

In the southern portion of sheet 4, where the quartzite is several tens of meters thick, the quartzite has a mean $\delta^{18}O$ value of 12.8‰ ($1\sigma < 0.1‰$, $n = 3$), and two quartz veins have values of 12.3 and 12.6‰. These values are similar to those of sheet 3 quartzite and veins, and have not appreciably exchanged with the surrounding basement gneisses or meteoric water. In contrast, in the more northeasterly located outcrops of sheet 4, where the quartzite horizon is very highly strained and only a few meters thick, two quartzite samples have lower values of 11.8 and 10.9‰. Whole rock values for three samples of felsic gneisses surrounding the quartzite are between 8.4 and 9.4‰. The quartz in felsic gneisses with whole rock values of 8–9‰ (typical values of granites and felsic gneisses, cf. Taylor 1974) is generally between 10 and 11‰ (cf. fig. 7 in Sharp *et al.* 1993). Therefore, where the quartzite horizon was very thin, isotopic exchange could have lowered the quartzite $\delta^{18}O$ values toward the basement quartz values. Results for sheet 5 support this interpretation, although we cannot rule out that the two lowest values in the quartzite are just primary protolith values for this part of the Heavitree Quartzite.

Thrust sheet 5

Quartzites of sheet 5 have a mean value of 11.5‰ ($1\sigma = 1.1‰$, $n = 13$), while three veins have values between 10.3 and 11.5‰. Whole rock $\delta^{18}O$ values of four felsic gneisses are ~8.3‰. The $\delta^{18}O$ values of sheet 5 quartzite and veins are in general 1.0–1.5‰ lower than samples analyzed from the other four thrust sheets of the duplex. As already mentioned, these values for quartz

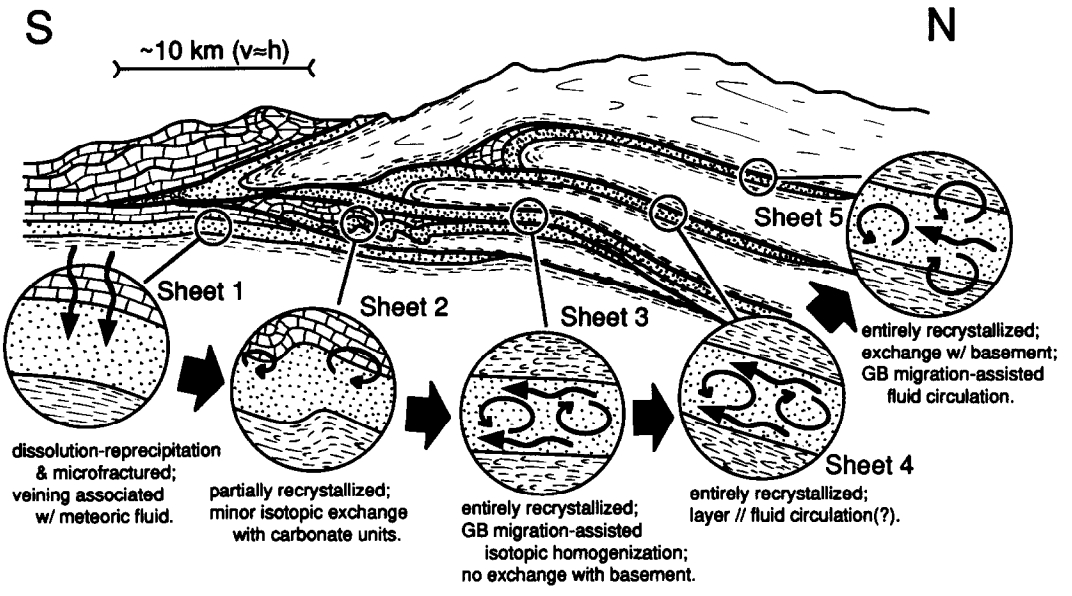

Fig. 7. Isotopic exchange and fluid pathways in evolving duplex as inferred from oxygen isotope data. Though meteoric fluids were involved in some vein formation of sheets 1 and 2, most of the duplex experienced very limited fluid flow in a relatively dry intracratonic environment. Some quartzite of sheet 5 exchanged isotopically with basement gneisses. The structural position and fluid-rock interaction of sheet 5 would have resembled those of sheet 2, 3, and then sheet 4 quartzite with subsequent imbrication of new thrusts. (Cross section is schematic.)

are similar to the $\delta^{18}O$ values of quartz in many felsic metamorphic rocks (Sharp *et al.* 1993). Given that sheet 5 quartzite is bounded both below and above by highly sheared felsic gneisses, fluids isotopically buffered by the gneisses could account for the lowering of the $\delta^{18}O$ values. Relatively low fluid/rock ratios on the order of 1.3–0.8 (closed and open system exchange, respectively; Taylor 1977) are required to account for the isotopic exchange of sheet 5 quartzite. The other basement rocks analyzed from sheet 5 (e.g. mafic rocks, felsic pegmatite) have $\delta^{18}O$ values typical for their rock types with no evidence for the extensive incursion of meteoric or isotopically-exotic fluids. This conclusion is supported by the δD value of −62‰ for neocrystallized white mica (cf. fig. 8 in Sharp *et al.* 1993).

Isotopically-rock dominated system

The isotopic data are consistent with the Ruby Gap duplex having formed and deformed ductilely under isotopically rock-dominated conditions (Fig. 7). Very little, if any, fluid could have been released during the low-grade metamorphism of already highly metamorphosed basement gneisses. Nor did the prograde metamorphism of the unmetamorphosed Proterozoic Heavitree Quartzite and Bitter Springs Formation provide much fluid. In addition, very little magmatism was associated with the Alice Springs orogeny (Shaw *et al.* 1984), eliminating a potential fluid source related to melt crystallization or the generation of hydrothermal convection systems. What little fluid was present in the orogen during formation of the Ruby Gap duplex could only have been due to the burial of water-bearing sediments during overthrusting of structurally higher nappes (Beach & Fyfe 1972), seismic pumping (Sibson 1981, McCaig 1988), or hydraulic pressure gradients resulting from surface uplift of a mountain belt overlying the orogen.

The two syntectonic vein arrays of sheets 1 and 2 with $\delta^{18}O$ values as low as 3‰ require that some meteoric fluids infiltrated the quartzite, possibly during the initial stages of deformation of each thrust sheet when they were incorporated into the duplex. However, the remainder of the isotopic data from Ruby Gap suggests that the interaction with meteoric water or other isotopically-disequilibrium fluids was minor. The scale of fluid advection responsible for most of the quartz veins must have been limited and not associated with large-scale midcrustal fluid circulation (e.g. Etheridge *et al.* 1983).

PROCESSES OF ISOTOPIC EXCHANGE

The following processes may explain the relations observed in the Heavitree Quartzite deformed in the Ruby Gap duplex: (i) apparent isotopic homogenization due to strain, and enhanced isotopic exchange associated with changes in grain shape and CPO; (ii) microfracturing and dissolution–reprecipitation; and (iii) dynamic recrystallization associated with dislocation creep. These processes are not unique to Ruby Gap but are typical in quartzite deformed under greenschist-grade conditions (e.g. Marjoribanks 1976, Bouchez 1977).

Strain, grain shape and CPO

During deformation, material particles are displaced relative to one another, affecting the distribution of

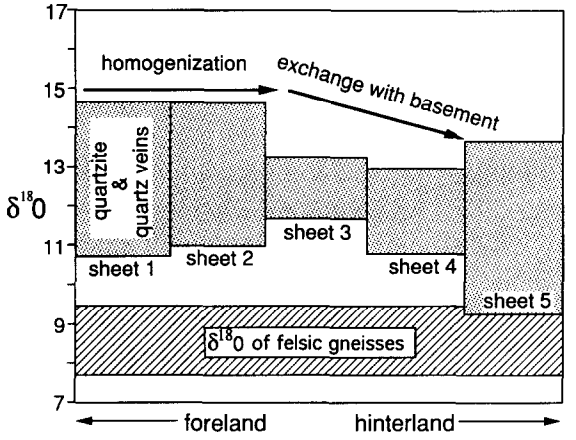

Fig. 8. Sheet 1 and 2 protolith $\delta^{18}O$ values of quartzite homogenized during deformation to form sheet 3 values. This isotopic homogenization corresponds to microstructural transition from partial recrystallization of sheets 1 and 2 to complete recrystallization of sheet 3 quartzite by grain boundary migration recrystallization. Some $\delta^{18}O$ values of sheet 5 quartzite have been depressed downward due to exchange with isotopically-lighter felsic basement gneisses.

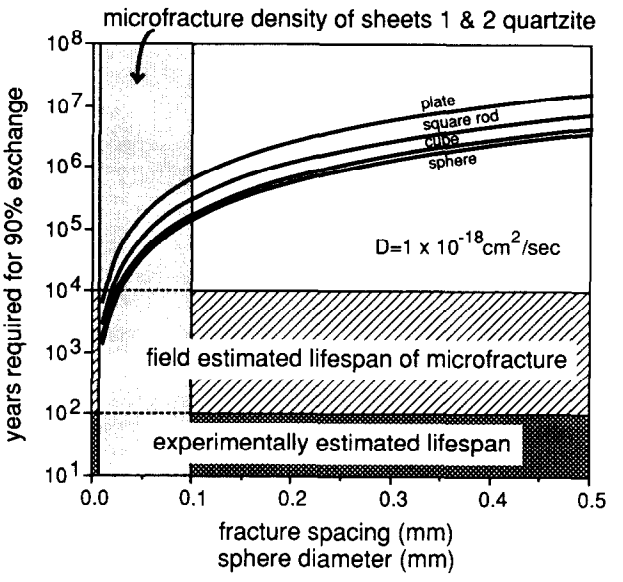

Fig. 9. Time required for isotopic exchange to proceed to 90% of equilibrium between solids of different geometries immersed in an isotopically-buffered fluid. Plate, square rod, and cube idealized fracture patterns formed by one, two and three orthogonal fracture sets, respectively. Experimental- and field-estimated lifespans of microfractures taken from literature (see text). Microfractures of Ruby Gap quartzite are not spaced closely enough to have resulted in significant isotopic exchange with a fracture-filling fluid even for relatively fast diffusion rates. Time required for isotopic exchange would be significantly shorter if dissolution and reprecipitation of quartz occurred within the microfractures.

isotopic heterogeneities. The higher the strain, the more likely it is that grains initially far apart, and potentially carrying different isotopic signatures, would be brought in close proximity, resulting in isotopic homogenization on the scale of the sample analyzed. This strain effect necessarily played a role on a centimeter scale in the Ruby Gap duplex, but is unlikely to have been dominant because it cannot explain homogenization on the scale of a whole sheet (as in sheet 3) or produce the shift in isotopic values in sheet 5 (Fig. 8).

On the scale of individual quartz grains, deformation had two consequences: (1) change in grain shape, from subspherical to ellipsoidal, resulting in a decrease of distance from rim to center and an increase in surface area to volume ratios; and (2) quartz *c*-axes preferentially oriented along the short axes of grains (Figs. 2b and 4), with diffusion parallel to the *c*-axis two orders of magnitude faster than diffusion parallel to the *a*-axis (Dennis 1984, Giletti & Yund 1984). Although these changes enhanced volume diffusion, they did not result in significant isotopic exchange during the relatively low temperature deformation of the Heavitree Quartzite.

Microfracturing and dissolution–reprecipitation

Microfracture networks are assumed to be one of the primary pathways of advecting fluid through deforming rocks (Walther & Orville 1982, Yardley 1984), but their relations to oxygen isotope exchange has been poorly studied. The typical microfracture density in sheets 1 and 2 of Ruby Gap is 10 fractures per millimeter. If these microfractures were filled by and exchanged with an isotopically buffered fluid for their entire lifetime (typical maximum 10,000 years, as estimated from Smith & Evans 1984, Brantley *et al.* 1990, Brantley 1992, Fisher & Brantley 1992), it can be shown that there would still be insignificant isotopic exchange by volume diffusion between the fluid and the fracture walls, even if a high coefficient of volume diffusion for oxygen in quartz is assumed ($D_{vol} = 10^{-18}$ cm^2/s; Giletti & Yund 1984, Farver & Yund 1991a). Only for a fracture density exceeding ~100 fractures per millimeter would volume diffusion associated with microfracturing become significant (Fig. 9). This trend is consistent with the observation that fractured quartz porphyroclasts have retained the $\delta^{18}O$ value of relatively undeformed quartz grains, except in high fracture density domains (40–100 fractures/mm), where quartz porphyroclasts show $\delta^{18}O$ values as low as 8‰. These lighter isotopic values might have resulted from diffusional exchange, though localized dissolution–reprecipitation during crack healing or the addition of new, isotopically light (~3‰) quartz that seals the microfractures was probably the dominant reason for the measured isotopic shift (Kirschner *et al.* 1993). The (re)precipitated quartz seals, which would have to be thicker than several microns to account for the $\delta^{18}O$ depletion, are not evident, however, under conventional optical and cathodoluminescence microscopy.

Oxygen in quartz isotopically exchanges with an aqueous fluid during the process of dissolution and reprecipitation (pressure solution). The isotopic value in the newly precipitated quartz can be drastically changed relative to that in the quartz source, depending on the relative isotopic compositions of the fluid and dissolving quartz, and the change in temperature between the time of dissolution and reprecipitation. In a situation analagous to mass transfer processes in metamorphic tectonites, quartz cementation of quartz arenites during compaction and low-temperature diagenesis can alter whole

rock $\delta^{18}O$ values up to several per mil (e.g. Fisher & Land 1986). In the quartzite of Ruby Gap, pressure solution has not homogenized the isotopic heterogeneity of sheets 1 and 2 quartzite even though up to 10% of the quartz might have locally gone through the pressure-solution cycle (visual estimate). It is impossible to quantify in the entirely recrystallized quartzite of thrust sheets 3–5 the percentage of quartz that participated in a pressure-solution cycle or the resulting isotopic exchange.

It is conceivable that microfracturing and dissolution–reprecipitation played an important role in isotopic exchange of thrust sheets 3–5. Transient microfracturing might have occurred during seismic events, and dissolution–reprecipitation might have accommodated the stress–strain incompatibilities at grain contacts during ductile deformation by dislocation creep. However, the effect of fracturing and mass transfer cannot be quantified because dynamic recrystallization has obliterated most physical traces of these processes.

Increased diffusivity due to dislocations

The production and migration of dislocations during deformation is known to increase bulk (volume) diffusion in metals, alkali halides, and silicates (Harrison 1960, Cohen 1970, Le Claire & Rabinovitch 1984, Yund *et al.* 1981, Yund *et al.* 1989). The dislocation density in the quartzite can be estimated from experimentally derived density–differential stress relations. Estimated differential stresses for the Heavitree Quartzite in the Ruby Gap duplex range from 10 to 200 MPa (data from Dunlap 1992 using the recrystallized grain size–stress relationship of Koch 1983). Dislocation densities in equilibrium with these stress levels are on the order of 10^6–10^9 cm^{-2} using the calibration of Weathers *et al.* (1979) and Kohlstedt & Weathers (1980).

Volume diffusion of the Heavitree Quartzite would have only increased by a factor of ~2–4 (Fig. 10; calculated using the equation of Hart 1957). This minor increase in bulk diffusion due to rapid diffusion through dislocations reflects the paucity of dislocations relative to undisturbed lattice area (i.e. adjacent dislocations are separated by several hundred unit cells at a dislocation density of 10^9 cm^{-2}; cf. Yund *et al.* 1981). This slight enhancement in bulk diffusion cannot account for the observed isotopic patterns in Ruby Gap unless the dislocation density in the quartz were several orders of magnitudes higher in sheets 3–5 relative to sheets 1 and 2 for the time necessary for significant isotopic exchange by diffusion. There is no reason to think this was ever the case, and it is in fact opposite to the decrease in dislocation density preserved from sheets 1–5.

Recrystallization and grain-boundary migration

Dynamically recrystallized grains are the product of either progressive subgrain rotation or nucleation and growth of new strain-free regions within otherwise strained grains (Poirier & Guillopé 1979, Poirier 1985,

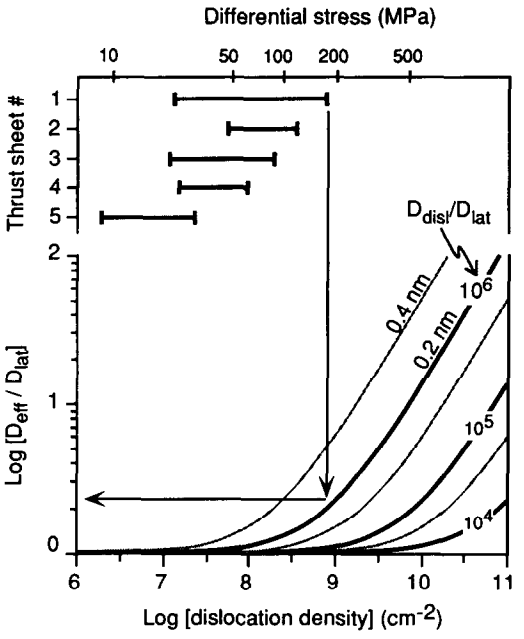

Fig. 10. Lower set of curves delineates theoretical relationship between dislocation density and enhanced bulk (effective) diffusion in quartz for dislocation pipe radii of 0.2–0.4 nm (solid and hatched lines, respectively) and diffusion coefficient ratios between dislocation and lattice diffusion of 10^4–10^6. Inferred equilibrium dislocation densities in quartzite from thrust sheets 1–5 range from 10^6–10^9 cm^{-2} corresponding to flow strengths of 10–200 MPa (stress levels from Dunlap 1992). Differential stresses probably never greatly exceeded 200 MPa during the quartzite deformation. Increase in bulk diffusion due to stationary dislocations would have been much less than one order of magnitude and cannot account for isotopic variations in quartzite between thrust sheets.

Urai *et al.* 1986, Drury & Urai 1990). The relative importance of these processes in recrystallization depends on the rates of dislocation production, grain-boundary migration and dislocation climb, which are principally a function of temperature, stress, strain rate and fluid involvement. Hirth & Tullis (1992) have identified three dislocation creep regimes of quartz aggregates in experimental deformation where temperature and strain rate were systematically varied. Grain-boundary migration recrystallization dominates deformation at lower temperatures or higher strain rates (thus higher stresses), where the rate of dislocation production is much greater than the recovery provided by dislocation climb, so that grain boundary migration recrystallization is the dominant recovery mechanism (regime 1). At higher temperatures or lower strain rates, recovery by climb keeps pace with dislocation production resulting in recrystallization by subgrain rotation (regime 2). At even higher temperatures or slower strain rates, recovery is accomplished by both grain-boundary migration and subgrain rotation recrystallization (regime 3).

There is evidence that these three regimes of dislocation creep were operative during deformation of the quartzite in Ruby Gap. Hirth *et al.* (1991) and Dunlap (1992), based on observations of microstructures in over 80 samples, have suggested that the quartzite in sheet 1 deformed predominantly in regime 1 conditions, the quartzite in sheet 2 deformed predominantly in regime 2, and the quartzite of sheets 3–5 in regime 3. These

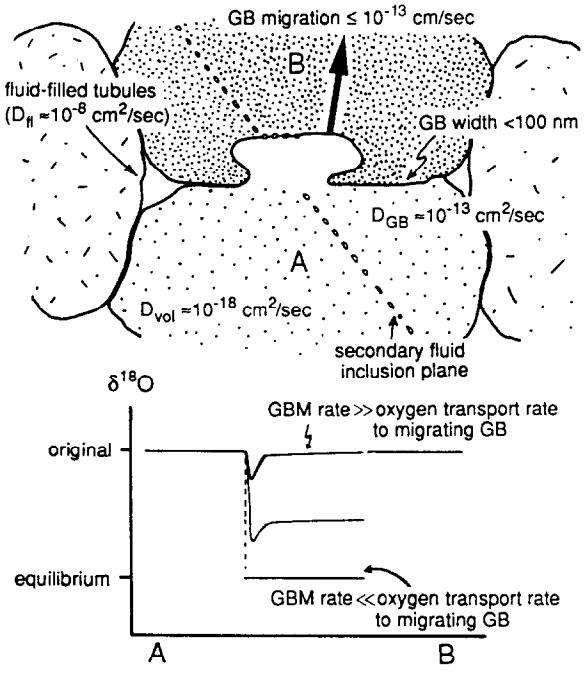

Fig. 11. Approximate diffusion and grain boundary migration rates for quartz at greenschist-facies conditions. Isotopic exchange between fluid and quartz is facilitated by grain-boundary migration. Each material point can be transferred many times across migrating boundaries during one orogenic event, leading to partial or complete isotopic equilibration. The effectiveness of this process depends, in part, on rate of boundary migration relative to oxygen transport rate to the grain boundary through adjacent fluid-filled grain boundary pores and tubules. Secondary fluid inclusions entrained in migrating boundary may enhance both boundary migration and oxygen diffusion rates.

conclusions, however, might only be appropriate in describing the late stages of deformation, especially for entirely recrystallized sheets 3–5, since grain-boundary migration could have overprinted earlier phases of subgrain rotation recrystallization (cf. Means & Ree 1988). Dynamic recrystallization resulted in grain-size reduction by one order of magnitude or more (Dunlap 1992), but did not produce the fine grainsize (<10 μm) for which exchange by volume diffusion would be significant.

It is only in sheets 3–5, where recrystallization in regime 3 was by grain boundary migration and subgrain rotation, that the $\delta^{18}O$ values were homogenized or shifted relative to undeformed protolith values. We propose that the *principal isotopic exchange process* in the quartzite of Ruby Gap, which resulted in the homogenization and depletion of sheets 3–5, occurred during recrystallization by grain-boundary migration when material was transferred across highly disordered grain boundaries.

The effectiveness of grain boundary migration recrystallization in affecting isotopic exchange depends on the rate of grain-boundary diffusion, the scale of isotopic heterogeneity, the presence and distribution of fluid, the effective width of the migrating grain boundary, the boundary migration rate, and the number of times a material point is transferred across a boundary (cf. Yund & Tullis 1991, Fig. 11). Oxygen self-diffusion along stationary quartz grain boundaries is four to six orders of magnitude faster than through grain interiors (e.g. $D_{gb} \approx 10^{-12}$ cm²/sec relative to $D_{vol} \approx 10^{-18}$ cm²/sec for 450°C; Farver & Yund 1991b). The rate of diffusion along migrating grain boundaries is probably of the same order of magnitude as that along stationary grain boundaries (Balluffi 1984). Fast grain-boundary diffusion rates can result in isotopic exchange along narrow (~1–10 nm wide; White & White 1981, Brady 1983, Joesten 1991) but long (μm–mm) grain boundaries. In the limit where the grain-boundary migration rate is zero, the extent of isotopic exchange is limited by the rates of grain-boundary and volume diffusion (Cahn & Balluffi 1979), and exchange will occur on a scale less than several centimeters for typical geologic conditions (Joesten 1991).

Only when grain boundaries are migrating can exchange occur over more significant distances. The presence of a grain shape fabric and the ubiquitous occurrence of mica enclosed in the center of recrystallized quartz indicates significant grain boundary movement during deformation of the Heavitree Quartzite, although it is impossible to constrain the number of times that material points have been traversed by grain boundaries based solely on these microstructures. The migration rate of a grain boundary is a linear function of the driving force times the grain-boundary mobility in the simplest case (cf. Nicolas & Poirier 1976, Poirier 1985). The driving force resulting from strain-energy gradients between adjacent grains can be estimated (i.e. ~10^2–10^4 N/m² for dislocation densities of 10^6–10^9 cm^{-2}, respectively; calculated using the appropriate values for quartz in the formulation of Nicolas & Poirier 1976, p. 86); however, as far as we know, there are no studies that have calculated the mobility of quartz grain boundaries related to strain-induced migration. Following a different approach, Prior *et al.* (1990) have estimated the velocity of strain-induced subgrain boundary migration to be on the order of 10^{-9}–10^{-11} μm/s, based on differences in quartz subgrain sizes around porphyroclasts in mylonites from New Zealand (temperature of deformation between ~300–500°C; Craw 1988; Prior 1988). At such velocities, (sub)grain boundaries would traverse 100 μm grains in 10^3–10^5 years. If similar velocities prevailed during a portion of the prolonged deformation of the Heavitree Quartzite, then material would have been transferred many times across migrating grain boundaries.

The efficiency of strain-induced grain boundary migration in affecting chemical exchange has been documented in deformation experiments of plagioclase aggregates composed of An_1 and An_{79} (Yund & Tullis 1991). Variable, intermediate plagioclase compositions were contained in the regions traversed by migrating boundaries. Similarly, Hay & Evans (1987) demonstrated for chemically-induced grain boundary migration in calcite bicrystals that transfer of material across one migrating boundary facilitated the approach but not the attainment of chemical equilibrium (see also fig. 4 in Cahn *et al.* 1979 for partial exchange in Cu–Au

alloy). Chemical equilibrium was more nearly attained in some regions that had been transferred across several grain boundaries.

The lateral extent of isotopic exchange in quartzite is limited by the transport of oxygen to the migrating boundaries, which is critically dependent on the distribution and interconnectivity of pore fluid. Oxygen transport would be predominantly by grain boundary diffusion in low-porosity (<1%), hydrostatically-stressed quartzite when the fluid is nonwetting (e.g. pure water below ~8 kbar, Watson & Brenan 1987, Holness 1992) and consequently confined to isolated pores (Farver & Yund 1992). In this case, isotopic exchange would be greater than for static grain boundaries but still be on the order of centimeters (Joesten 1991). Aqueous fluids above 8 kbar pressures can wet quartz and form an interconnected tubule network along three-grain junctions in the quartzite (Watson & Brenan 1987, LaPorte & Watson 1991, Holness 1992). Replenishment of oxygen to the migrating interface would be significantly enhanced by the presence of this fluid-filled network (Farver & Yund 1992). Isotopic exchange would be limited to the scale of meter(s) if the fluid is static (Fletcher 1982, Rubie & Thompson 1985) and possibly kilometers if the fluid is advecting.

The time required to obtain equilibrium wetting angle and pore shape geometry is on the order of hours to days, much shorter than the time required for significant movement of grain boundaries or alteration of pore geometry due to dislocation creep. Given this large disparity in rates between competing processes (Watson & Brenan 1987), the fluid distribution and pore geometry in undeformed quartzite and in quartzite undergoing dislocation creep and recrystallization are probably similar. Migrating boundaries are quite effective, however, in concentrating intracrystalline fluid inclusions (Kerrich 1976, Wilkins & Barkas 1978) and may contain more fluid lenses than stationary boundaries. The collection of fluid-filled lenses would effectively increase diffusivity along the grain boundaries and thus enhance the effectiveness of isotopic exchange during grain-boundary migration with a possible positive feedback on the migration rate (Urai 1987).

The variation in $\delta^{18}O$ whole rock values of sheets 3–5 (Fig. 6) may be related to heterogeneous fluid migration from the basement gneisses into the mylonitized quartzite. The recrystallized samples, which retain protolith $\delta^{18}O$ values of 12–13‰, must not have been in extensive contact with fluids from the basement gneisses. The recrystallized samples with isotopically-depleted values of 10–11‰ must have extensively exchanged with such fluids. The heterogeneity of $\delta^{18}O$ in quartz mylonites that have undergone extensive grain-boundary migration recrystallization is only possible where the deformation occurred in a relatively dry environment such as the intracratonic Alice Springs Orogen.

CONCLUSIONS

The results of oxygen isotope analyses of Heavitree Quartzite, quartz veins, and basement gneisses of Ruby Gap duplex are consistent with deformation having occurred in a relatively closed system with minor fluid advection. Isotopic exchange and homogenization in the mylonitized quartzite are correlated with intensity of deformation and recrystallization and cannot be accounted for solely by juxtaposition of different isotopic reservoirs due to strain and shear displacement. Diffusional exchange between quartz grains and fluid-filled microfractures and grain boundary pores is also too sluggish at the temperatures of deformation (300–400 °C) to explain homogenization, unless isotopically-buffered fluids resided in these pores for millions of years or oxygen self-diffusion in quartz is faster than predicted experimentally.

Dissolution–reprecipitation probably played an important role in isotopic exchange of the quartzite mylonites by accommodating stress–strain incompatibilities at grain contacts during ductile deformation by dislocation creep. However, the effect of mass transfer cannot be quantified because dynamic recrystallization has obliterated most physical traces of these processes. Where dynamic recrystallization was accompanied by grain boundary migration, significant isotopic exchange occurred. Isotopic exchange was probably facilitated when material was transferred across the highly disordered and possibly fluid-bearing migrating grain boundaries. Although only partial isotopic equilibration might have occurred during any single transfer across a migrating boundary, individual material points in the recrystallized quartz were probably transferred across many migrating boundaries during the course of the orogeny, resulting in significant isotopic exchange. This commonly overlooked phenomenon is probably an important mechanism of isotopic exchange in rocks undergoing dynamic recrystallization.

Acknowledgements—We thank Jim Dunlap, Greg Hirth and Shun Karato for many useful discussions on the processes of quartzite deformation. Mark Brandon, Jim Dunlap, Emi Ito and Jan Tullis made many constructive comments on the paper. We thank Steven Wojtal for the editorial handling of this paper. Support from National Science Foundation grants EAR-8720755 (CT) and EAR-9005583 (CT and RTG) are gratefully acknowledged.

REFERENCES

Balluffi, R. W. 1984. Grain boundary diffusion mechanisms in metals. In: *Diffusion in Crystalline Solids* (edited by Murch, G. E. & Nowick, A. S.). Academic Press, Orlando, 319–377.

Beach, A. & Fyfe, W. S. 1972. Fluid transport and shear zones at Scourie, Sutherland: evidence for overthrusting? *Contr. Miner. Petrol.* **36**, 175–180.

Borthwick, J. & Harmon, R. S. 1982. A note regarding ClF_3 as an alternative to BrF_5 for oxygen isotope analyses. *Geochim. cosmochim. Acta* **46**, 1665–1668.

Bouchez, J. L. 1977. Plastic deformation of quartzites at low temperature in an area of natural strain gradient (Angers, France). *Tectonophysics* **39**, 25–80.

Bouchez, J. L., Lister, G. S. & Nicolas, A. 1983. Fabric asymmetry and shear sense in movement zones. *Geol. Rund.*, **72**, 401–419.

Boyer, S. E. & Elliott, D. 1982. Thrust systems. *Bull. Am. Ass. Petrol. Geol.* **66**, 1196–1230.

Brady, J. B. 1983. Intergranular diffusion in metamorphic rocks. *Am. J. Sci.* **283-A**, 181–200.

Brantley, S. L. 1992. The effect of fluid chemistry on quartz microcrack lifetimes. *Earth Planet. Sci. Lett.* **113**, 145–156.

Brantley, S. L., Evans, B., Hickman, S. H. & Crear, D. A. 1990. Healing of microcracks in quartz: implications for fluid flow. *Geology* **18**, 136–139.

Burg, J. P. 1986. Quartz shape fabric variations and *c*-axis fabrics in a ribbon-mylonite: arguments for an oscillating foliation. *J. Struct. Geol.* **8**, 123–131.

Cahn, J. W. & Bulluffi, R. W. 1979. On diffusional mass transport in polycrystals containing stationary or migrating grain boundaries. *Scr. Met.* **13**, 499–502.

Cahn, J. W., Pan, J. D. & Bulluffi, R. W. 1979. Diffusion induced grain boundary migration. *Scr. Met.* **13**, 503–509.

Clarke, D. 1979. Heavitree quartzite stratigraphy and structure near Alice Springs, N.T. Northern Territory Geological Survey (Australia), Report 79/23.

Cohen, M. 1970. Self diffusion during plastic deformation. *Trans. Japan Inst. Metals* **11**, 145–151.

Collins, W. J. & Teyssier, C. 1989. Crustal scale ductile fault systems in the Arunta Inlier, central Australia. *Tectonophysics* **158**, 49–66.

Craw, D. 1988. Shallow-level metamorphic fluids in a high uplift rate metamorphic belt; Alpine Schist, New Zealand. *J. metamorphic Geol.* **6**, 1–16.

Dennis, P. F. 1984. Oxygen self-diffusion in quartz under hydrothermal conditions. *J. geophys. Res.* **89**, 4047–4057.

Drury, M. R. & Urai, J. L. 1990. Deformation-related recrystallization processes. *Tectonophysics* **172**, 235–253.

Dunlap, W. J. 1992. Structure, kinematics, and cooling history of the Arltunga nappe complex, central Australia. Unpublished Ph.D. dissertation, University of Minnesota, Minneapolis.

Dunlap, W. J., Teyssier, C., McDougall, I. & Baldwin, S. 1991. Ages of deformation from K/Ar and $^{40}Ar/^{39}Ar$ dating of white micas. *Geology* **19**, 1213–1216.

Dunlap, W. J., Teyssier, C., McDougall, I., & Baldwin, S. In press. Thermal and structural evolution of intracratonic Arltunga Nappe Complex, central Australia. *Tectonics*.

Etheridge, M. A., Wall, V. J. & Vernon, R. H. 1983. The role of the fluid phase during regional metamorphism and deformation. *J. metamorph. Geol.* **1**, 205–226.

Farver, J. R. & Yund, R. A. 1991a. Oxygen diffusion in quartz: dependence on temperature and water fugacity. *Chem. Geol.* **90**, 55–77.

Farver, J. R. & Yund, R. A. 1991b. Measurement of oxygen grain boundary diffusion in natural, fine-grained, quartz aggregates. *Geochim. cosmochim. Acta* **55**, 1597–1607.

Farver, J. R. & Yund, R. A. 1992. Oxygen diffusion in a fine-grained quartz aggregate with wetted and nonwetted microstructures. *J. geophys. Res.* **97**, 14,017–14,029.

Fisher, D. M. & Brantley, S. L. 1992. Models of quartz overgrowth and vein formation: deformation and episodic fluid flow in an ancient subduction zone. *J. geophys. Res.* **97**, 20043–20061.

Fisher, R. S. & Land, L. S. 1986. Diagenetic history of Eocene Wilcox sandstones, South-Central Texas. *Geochim. cosmochim. Acta* **50**, 551–561.

Fletcher, R. C. 1982. Coupling of diffusional mass transport and deformation in a tight rock. *Tectonophysics* **83**, 275–291.

Forman, D. J. 1971. The Arltunga Nappe Complex, MacDonnell Ranges, Northern Territory. *J. geol. Soc. Aust.* **18**, 173–182.

Forman, D. J., Milligan, E. N. & McCarthy, W. R. 1967. Regional geology and structure of the north-east margin, Amadeus Basin, central Australia. *Bur. Min. Res., Aust. Rec.* **1967/103**.

Frey, M., Hunziker, J. C., O'Neil, J. R. & Schwander, H. W. 1976 Equilibrium–disequilibrium relations in the Monte Rosa Granite, Western Alps: petrological, Rb-Sr, and stable isotope data. *Contr. Miner. Petrol.* **55**, 147–179.

Giletti, B. J. & Yund, R. A. 1984. Oxygen diffusion in quartz. *J. geophys. Res.* **89**, 4039–4046.

Gray, D. R., Gregory, R. T. & Durney, D. W. 1991. Rock-buffered fluid-rock interaction in deformed quartz-rich turbidite sequences, eastern Australia. *J. geophys. Res.* **96**, 19681–19704.

Harrison, L. G. 1960. Influence of dislocations on diffusion kinetics in solids with particular reference to the alkali halides. *Trans. Faraday Soc.* **57**, 1191–1199.

Hart, E. W. 1957. On the role of dislocations in bulk diffusion. *Acta Metall.* **5**, 597.

Hay, R. S. & Evans, B. 1987. Chemically induced grain boundary migration in calcite: temperature dependence, phenomenology, and possible applications to geologic systems. *Contr. Miner. Petrol.* **97**, 127–141.

Hirth, G. & Tullis, J. 1992. Dislocation creep regimes in quartz aggregates. *J. Struct. Geol.* **14**, 145–159.

Hirth, G., Dunlap, W. J. & Teyssier, C. 1991. Analysis of dislocation creep microstructures in Heavitree Quartzite deformed in the Ruby Gap duplex, central Australia. *Geol. Soc. Am. Abs. w. Progr.* **23**, 425.

Holness, M. B. 1992. Equilibrium dihedral angles in the system quartz-CO_2-H_2O-NaCl at 800°C and 1–15 kbar: the effects of pressure and fluid composition on the permeability of quartzites. *Earth Planet. Sci. Lett.* **114**, 171–184.

Joesten, R. 1991. Grain-boundary diffusion kinetics in silicate and oxide minerals. In: *Diffusion, Atomic Ordering, and Mass Transport* (edited by Ganguly, J.). Springer-Verlag, NY, 345–395.

Keith, M. L. & Weber, J. N. 1964. Carbon and oxygen isotopic composition of selected limestones and fossils. *Geochim. cosmochim. Acta* **28**, 1787–1816.

Kerrich, R. 1976. Some effects of tectonic recrystallisation on fluid inclusions in vein quartz. *Contr. Miner. Petrol.* **59**, 195–202.

Kirschner, D. L. & Teyssier, C. 1992. Deformation history of the White Range Duplex, central Australia, with implications for fold reorientation. *Aust. J. Earth Sci.* **39**, 441–456.

Kirschner, D. L., Sharp, Z. D. & Teyssier, C. P. 1993. Vein growth mechanisms and fluid sources revealed by oxygen isotope laser microprobe. *Geology* **21**, 85–88.

Koch, P. 1983. Rheology and microstructures of experimentally deformed quartz aggregates. Unpublished Ph.D. dissertation, University of California, Los Angeles.

Kohlstedt, D. L. & Weathers, M. S. 1980. Deformation-induced microstructures, paleopiezometers, and differential stresses in deeply eroded fault zones. *J. geophys. Res.* **85**, 6269–6285.

LaPorte, D. & Watson, E. B. 1991. Direct observation of near-equilibrium pore geometry in synthetic crustal quartzites at 600°–800°C and 2–10.5 kbars. *J. Geol.* **99**, 873–878.

Le Claire, A. D. & Rabinovitch, A. 1984. The mathematical analysis of diffusion in dislocations. In: *Diffusion in Crystalline Solids* (edited by Murch, G. E. & Nowick, A. S.). Academic Press, Orlando, 257–318.

Lister, G. S. & Snoke, A. W. 1984. *S–C* mylonites. *J. Struct. Geol.* **6**, 617–638.

McCaig, A. M. 1988. Deep fluid circulation in fault zones. *Geology* **16**, 867–870.

McCrea, J. M. 1950. On the isotopic chemistry of carbonates and a paleotemperature scale. *J. Chem. Physics* **18**, 849–857.

Marjoribanks, R. W. 1976. The relationship between microfabric and strain in a progressively deformed sequence from central Australia. *Tectonophysics* **32**, 269–293.

Means, W. D. & Ree, J. H. 1988. Seven types of subgrain boundaries in octachloropropane. *J. Struct. Geol.* **10**, 765–770.

Nicolas, A. & Poirier, J. P. 1976. *Crystalline Plasticity and Solid State Flow in Metamorphic Rocks*. John Wiley & Sons, London.

O'Neil, J. R. & Taylor, H. P., Jr. 1969. Oxygen isotope equilibrium between muscovite and water. *J. geophys. Res.* **74**, 6,012–6,022.

Poirier, J. P. 1985. *Creep of Crystals*. Cambridge University Press, Cambridge.

Poirier, J. P. & Guillopé, M. 1979. Deformation induced recrystallization of minerals. *Bull. Mineral.* **102**, 67–74.

Prior, D. J. 1988. Deformation processes in the Alpine Fault Mylonites, South Island, New Zealand. Unpublished Ph.D. dissertation, University of Leeds, England.

Prior, D. J., Knipe, R. J. & Handy, M. R. 1990. Estimates of the rates of microstructural changes in mylonites. In: *Deformation Mechanisms, Rheology, and Tectonics* (edited by Knipe, R. J. & Rutter, E. H.). *Spec. Publs geol. Soc.* **54**, 309–319.

Rubie, D. C. & Thompson, A. B. 1985. Kinetics of metamorphic reactions at elevated temperatures and pressures. In: *Metamorphic Reactions, Kinetics, Textures and Deformation* (edited by Thompson, A. B. & Rubie, D. C.). Springer-Verlag, NY, 27–79.

Sharp, Z. D. 1990. A laser-based microanalytical method for the *in situ* determination of oxygen isotope ratios in silicates and oxides. *Geochim. cosmochim. Acta* **54**, 1353–1357.

Sharp, Z. D. 1992. In situ laser microprobe techniques for stable isotope analysis. *Chem. Geol.* **101**, 3–19.

Sharp, Z. D. & Kirschner, D. L. 1994. Quartz-calcite oxygen isotope thermometry: a calibration based on natural isotopic variations. *Geochim. cosmochim. Acta* **58**, 4491–4501.

Sharp, Z. D., Essene, E. J. & Hunziker, J. L. 1993. Stable isotope

geochemistry and phase equilibria of coesite-bearing whiteschists, Dora Maira Massif, western Alps. *Contr. Miner. Petrol.* **114**, 1–12.
Shaw, R. D., Stewart, A. J., Yar Khan, M. & Funk J. L. 1971. Progress reports on detailed studies in the Arltunga Nappe Complex, Northern Territory. *Bur. Min. Res., Aust. Rec.* **1971/66**.
Shaw, R. D., Stewart, A. J., & Black, L. P. 1984. The Arunta Inlier: a complex insialic mobile belt in central Australia. Part 2: Tectonic history. *Aust. J. Earth Sci.* **31**, 457–484.
Sibson, R. H. 1981. Fluid flow accompanying faulting: field evidence and models. In: *An Internal Review* (edited by Simpson, D. W. & Richards, P. G.). *Am. Geophys. Un. Maurice Ewing Series* **4**, 493–503.
Smith, D. L. & Evans, B. 1984. Diffusional crack healing in quartz. *J. geophys. Res.* **89**, 4125–4135.
Stewart, A. J. 1971. Potassium-argon dates from the Arltunga Nappe Complex, Northern Territory. *J. geol. Soc. Aust.* **17**, 205–211.
Taylor, H. P., Jr. 1974. The application of oxygen and hydrogen isotope studies to problems of hydrothermal alteration and ore deposition. *Econ. Geol.* **69**, 843–883.
Taylor, H. P., Jr. 1977. Water/rock interactions and the origin of H_2O in granitic batholiths. *J. geol. Soc. Lond.* **133**, 509–558.
Teyssier, C. 1985. A crustal thrust system in an intracratonic tectonic environment. *J. Struct. Geol.* **7**, 689–700.
Urai, J. L. 1987. Development of microstructure during deformation of carnallite & bischofite in transmitted light. *Tectonophysics* **135**, 251–263.
Urai, J. L., Means, W. D. & Lister, G. S. 1986. Dynamic recrystallization of minerals. In: *Minerals and Rock Deformation: Laboratory Studies (Paterson Volume)* (edited by Heard, H. C. & Hobbs, B. E.). *Am. Geophys. Union Monogr.* **36**, 161–199.
Vennemann, T. W. & O'Neil, J. R. 1993. A simple and inexpensive method of hydrogen isotope and water analyses of minerals and rocks based on zinc reagent. *Chem. Geol.* **103**, 227–234.
Walther, J. & Orville, P. 1982. Volatile production and transport in regional metamorphism. *Contr. Miner. Petrol.* **79**, 252–257.
Watson, E. B. & Brenan, J. M. 1987. Fluids in the lithosphere, 1. Experimentally-determined wetting characteristics of CO_2–H_2O fluids and their implications for fluid transport, host-rock physical properties, and fluid inclusion formation. *Earth Planet. Sci. Lett.* **85**, 497–515.
Weathers, M. S., Cooper, R. F., Kohlstedt, D. L. & Bird, J. M. 1979. Differential stress determined from deformation-induced microstructures of the Moine Thrust zone. *J. geophys. Res.* **84**, 7495–7509.
White, J. C. & White, S. H. 1981. On the structure of grain boundaries in tectonites. *Tectonophysics* **78**, 613–628.
Yardley, B. 1984. Fluid migration and veining in the Connemara Schists, Ireland. In: *Fluid-Rock Interactions during Metamorphism* (edited by Walther, J. V. & Wood, B. J.). Springer-Verlag, NY, 109–131.
Yar Khan, M. 1972. The structure and microfabric of a part of the Arltunga Nappe Complex, central Australia. Unpublished Ph.D. dissertation, Australian National University, Canberra.
Yund, R. A. & Tullis, J. 1991. Compositional changes of minerals associated with dynamic recrystallization. *Contr. Miner. Petrol.* **108**, 346–355.
Yund, R. A., Smith, B. M. & Tullis, J. 1981. Dislocation-assisted diffusion of oxygen in albite. *Physics Chem. Minerals* **7**, 185–189.
Yund, R. A., Quigley, J. & Tullis, J. 1989. The effect of dislocations on bulk diffusion in feldspars during metamorphism. *J. metamorph. Geol.* **7**, 337–341.

APPENDIX 1

Analytical methods and errors

Conventional oxygen isotope analyses of ground rock powder were performed in the stable isotope laboratory at Monash University (Australia). Standard procedures were used in extracting oxygen from silicates by reaction with ClF_3 and converting to CO_2 (Borthwick & Harmon 1982). The standard used during the analyses of these samples was the Caltech Rose Quartz (accepted value 8.45‰) which gave a $\delta^{18}O$ value of 8.43‰ ± 0.08‰ (44 analyses). Carbonate samples were analysed following the conventional phosphoric acid method of McCrea (1950). The $\delta^{18}O$ values are presented in terms of standard mean ocean water V-SMOW.

Additional powder and in-situ oxygen isotope analyses were made at the Université de Lausanne (Switzerland) following the procedures of Sharp (1990, 1992). A 20 W CO_2 laser was used to heat ~1 mg powder sample and to produce 150–300 μm diameter holes in ~200 μm thick plates in a BrF_5 atmosphere. The liberated oxygen was cryogenically purified, converted to CO_2 by combustion of a heated carbon rod using a platinum catalyst and introduced directly on-line to the micro-inlet system of the mass spectrometer. An inhouse quartz standard or NBS-28 quartz standard was analyzed for every three or four powder samples analyzed. Data are adjusted to agree with a NBS-28 $\delta^{18}O$ value of 9.6‰, with a 1σ error of 0.17‰ (35 analyses). The long term analytical precision of the in-situ data is difficult to assess since no standard quartz plate was analyzed *in situ* during the course of this study. Although reproducibility of analyses for one microstructurally homogeneous sample (R674) in this study is better than 0.1‰ (3 analyses), a conservative estimate for the 1σ error for in-situ analyses is ±0.2–0.4‰. Temperatures were calculated for the oxygen isotope fractionations between quartz and white mica by combining the quartz–water fractionation of Sharp & Kirschner (1994) with the muscovite-water fractionation of O'Neil & Taylor (1969).

Hydrogen isotope analyses were made on pure mica separates at the Université de Lausanne following the procedure of Vennemann & O'Neil (1993). The ~20 mg samples were evacuated at 180°C for 4–12 h to remove adsorbed water. Samples were then melted, and water and other condensible gases were frozen on a liquid nitrogen cold trap. Evolved H_2 was converted to H_2O by reaction with a heated CuO furnace. The H_2O was separated from other gases cryogenically and frozen in silica glass tubes with ~50 mg of zinc metal. The tubes were sealed and reacted at 480°C for 30 min to quantitatively convert H_2O to H_2 via oxidation of the zinc. The hydrogen gas was introduced directly into the inlet system of the mass spectrometer with a simple cracking device. The resulting values are relative to standard mean ocean water V-SMOW, and adjusted to NBS-30 biotite standard (accepted δD value of 65‰; 1σ = 6‰ for set of analyses).